

Shape shifting: The multiple conformational substates of the PTEN N-terminal PIP₂-binding domain

Jennifer E. Dawson^{1,2}  | Iris Nira Smith^{1,2}  | William Martin¹ |
Krishnendu Khan³  | Feixiong Cheng^{1,2,4}  | Charis Eng^{1,2,3,5,6,7} 

¹Genomic Medicine Institute, Lerner Research Institute, Cleveland Clinic, Cleveland, Ohio, USA

²Cleveland Clinic Lerner College of Medicine, Case Western Reserve University, Cleveland, Ohio, USA

³Department of Cardiovascular and Metabolic Sciences, Lerner Research Institute, Cleveland Clinic, Cleveland, Ohio, USA

⁴Case Comprehensive Cancer Center, Case Western Reserve University School of Medicine, Cleveland, Ohio, USA

⁵Taussig Cancer Institute, Cleveland Clinic, Cleveland, Ohio, USA

⁶Department of Genetics and Genome Sciences, Case Western Reserve University School of Medicine, Cleveland, Ohio, USA

⁷Department of Computational and Systems Biology, School of Medicine, University of Pittsburgh, Pittsburgh, Pennsylvania, USA

Correspondence

Charis Eng, Cleveland Clinic, 9500 Euclid Avenue, NE-50, Cleveland, OH 44195, USA.

Email: engc@ccf.org

Funding information

Ambrose Monell Cancer Genomic Medicine Fellowship; Ambrose Monell Foundation (PTEN-Switch Grant); National Institute of General Medical Sciences, Grant/Award Number: 1K99GM143552-01; National Institute on Aging, Grant/Award Numbers: R01AG066707, U01AG073323; National Institutes of Health, Grant/Award Number: 1S10OD023436-01; Ohio Supercomputing Center, Grant/Award Number: PCCF0020

Review Editor: Nir Ben-Tal

Abstract

The Phosphatase and TENsin homolog deleted on chromosome 10 (*PTEN*) is a chief regulator of a variety of cellular processes including cell proliferation, migration, growth, and death. It is also a major tumor suppressor gene that is frequently mutated or lost under cancerous conditions. *PTEN* encodes a dual-specificity (lipid and protein) phosphatase that negatively regulates the PI3K/AKT/mTOR signaling pathway where the PIP₂-binding domain (PBD) regulates the lipid phosphatase function. Unfortunately, despite two decades of research, a full-length structure of *PTEN* remains elusive, leaving open questions regarding *PTEN*'s disordered regions that mediate protein stability, post-translational modifications, protein–protein interactions, while also hindering the design of small molecules that can regulate *PTEN*'s function. Here, we utilized a combination of crosslinking mass spectrometry, in silico predicted structural modeling (including AlphaFold2), molecular docking, molecular dynamics simulations, and residue interaction network modeling to obtain structural details and molecular insight into the behavior of the PBD of *PTEN*. Our study shows that the PBD exists in multiple conformations which suggests its ability to regulate *PTEN*'s variety of functions. Studying how these specific conformational substates contribute to *PTEN* function is imperative to defining its function in disease pathogenesis, and to delineate ways to modulate its tumor suppressor activity.

Jennifer E. Dawson and Iris Nira Smith contributed equally to this study.

This is an open access article under the terms of the Creative Commons Attribution-NonCommercial-NoDerivs License, which permits use and distribution in any medium, provided the original work is properly cited, the use is non-commercial and no modifications or adaptations are made.

© 2022 The Authors. *Protein Science* published by Wiley Periodicals LLC on behalf of The Protein Society.

KEYWORDS

AlphaFold, crosslinking mass spectrometry, integrative structural modeling, molecular docking, molecular dynamics simulations, PTEN, residue interaction network, RoseTTAFold

1 | INTRODUCTION

PTEN is one of the most frequently somatically mutated tumor suppressor genes in a wide spectrum of human cancers.^{1–4} *PTEN* encodes a dual-specificity (lipid and protein) phosphatase that inhibits the PI3K/AKT/mTOR signaling pathway, thereby controlling a plethora of cellular processes. The protein antagonizes the pathway by dephosphorylating the lipid phosphatidylinositol (3,4,5)-triphosphate (PIP₃) to phosphatidylinositol (4,5)-bisphosphate (PIP₂).^{1–3} Individuals with germline *PTEN* mutations are diagnosed with *PTEN* hamartoma tumor syndrome (PHTS) characterized by high risks of early-onset breast, thyroid, and other cancers.

The N-terminal tail of *PTEN* (or the PIP₂-binding domain, PBD) is a critical regulatory region involved in the enzymatic activation of *PTEN*. Residues 6–15 of PBD bind PIP₂^{5,6} and activate *PTEN* lipid phosphatase function,^{5,7,8} particularly residues K13, R14, and R15.⁹ In cells, PIP₂ binding helps recruit *PTEN* to the membrane,¹⁰ as well as enhancing its activity.¹¹ Decreased *PTEN* phosphatase activity in the cytoplasm suggests that the exchange between multiple *PTEN* conformations controls its phosphatase activity: a high activity conformation at the membrane bound to PIP₂, and lower activity and inactive conformations in solution.¹² The exchange between low and high activity *PTEN* in solution is affected by K13A and the *PTEN*-L isoform, which alter PBD and perturb *PTEN* phosphatase function.¹³ The *PTEN* PBD is predicted to be intrinsically disordered^{14,15} and this region is missing or incomplete in X-ray crystal structures,^{16–18} suggesting a dynamic region that could adopt multiple conformations.

Integrative structural modeling combines information from multiple sources to solve structures that would not otherwise be obtainable.^{19,20} Critical regulatory regions in *PTEN*—PBD, the intrinsically disordered region, and the C-terminal tail—are missing or incomplete in X-ray structures.^{16–18} NMR reveals that PBD binds to the rest of *PTEN* homolog VSP.¹⁸ Here, we combine experimental (crosslinking mass spectrometry or XL-MS), computational in silico protein prediction methods (AlphaFold2, RoseTTAFold, and I-TASSER), and molecular dynamics methods to determine the multiple conformational states of the *PTEN* PBD. We show that the PBD is a “shape shifter” that can exist in multiple conformational states with its positioning affecting the *PTEN* catalytic residues.

2 | RESULTS

2.1 | Multiple observed and predicted PBD intermolecular binding sites on PTEN

Impressive improvements have been made recently in protein structure prediction. In previous work, we constructed a full-length model of *PTEN*²¹ using I-TASSER.^{22,23} Now, taking advantage of next-generation Deep Machine Learning methods, we have constructed full-length models of *PTEN* using AlphaFold2^{24–26} and RoseTTAFold.²⁷ Intriguingly, each of these methods predicted the PIP₂-binding domain (PBD) in a different conformational state (Figure 1a, Figure S1 and Table S1 for model quality assessment and reproducibility of PBD orientation). An α -helix occupies the first ~10 residues in these structures with the remaining residues adopting a loop and short two-strand β -sheet. PBD's from the AlphaFold2 and RoseTTAFold models, and the partial PBD from a recent crystal structure¹⁸ (PDBID 7JUL), are present near the *PTEN* catalytic residues in the phosphatase domain (PD). The RoseTTAFold PBD overlays best with the partial 7JUL PBD, but the AlphaFold2 helix is bound in a different orientation. In contrast, the I-TASSER predicted PBD is remote from the catalytic residues.

PBD conformational states can be rationalized by patterns of amino acid residue types and sequence conservation. The I-TASSER PBD binds to a large patch of hydrophobic and aromatic residues (Figure S3a). In contrast, charged residues are observed on either end of the AlphaFold2 helix with a potential salt-bridge between K13 and D24, suggesting a more electrostatic driven interaction (Figure S3b). Based on sequence conservation and binding interface prediction methods (ConSurf^{28–31} and CPORT³²), the AlphaFold2 and RoseTTAFold PBD helices bind to highly conserved regions that are predicted to be binding hotspots, while the I-TASSER helix lies in a more variable region at the periphery of the predicted interface (Figure S3c,d). Overall, the patterns of amino acids, conservation, and interface predictions offer a large potential area for PBD binding to the PD, stretching from the catalytic residues, up toward the “top” of the PD.

2.2 | Predicted full-length PTEN structures do not satisfy all experimental XL-MS crosslinks

AlphaFold2, RoseTTAFold, and I-TASSER each predict different PBD conformational states. To confirm which

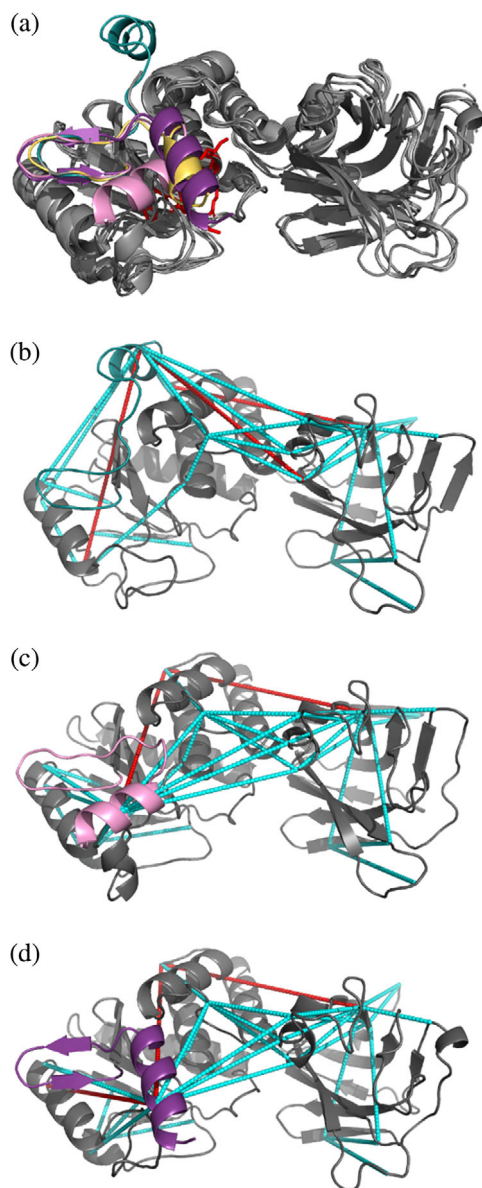


FIGURE 1 Testing multiple predicted PIP₂-binding domain (PBD) binding orientations with experimental XL-MS crosslinks. (a) X-ray structures of truncated PTEN (PBDID 1D5R and 7JUL) overlaid with the full-length PTEN predicted by I-TASSER, AlphaFold2, and RoseTTAFold. The phosphatase (PD) and C2 domains are in gray with the intrinsically disordered region and C-terminal tail removed for clarity where applicable. The catalytic residues are shown in red in stick representation. The PBD (in teal, residues 1–24 with linker) predicted by I-TASSER interacts with the top of the PTEN PD, while the PBD's predicted by AlphaFold2 and RoseTTAFold are in pink and purple, respectively. The partial PBD (residues 7–24) from the 7JUL X-ray structure is shown in gold. The AlphaFold2, RoseTTAFold, and 7JUL PBD are by the catalytic residues. (b–d) XL-MS crosslinks mapped onto PTEN structure. C α –C α distances within the effective length of the crosslinker (≤ 30 Å for DSSO, ≤ 45 Å for BMSO) are indicated with cyan dashed lines and those that are too long as red dashed lines. (b) I-TASSER PTEN structure. (c) AlphaFold2 PTEN structure. (d) RoseTTAFold PTEN structure. As before, the I-TASSER, AlphaFold2, and RoseTTAFold PBD are in teal, pink, and purple, respectively

model predicts the most accurate PTEN structure, crosslinking mass spectrometry (XL-MS) was performed with DSSO, which chemically crosslinks solvent-exposed proximal lysine residues³³ and BMSO that crosslinks proximal cysteines.³⁴ The effective (C α –C α) lengths of these crosslinks are 30 Å and 45 Å, respectively,^{34–36} offering a way of testing the plausibility of predicted structures. Thirty-one crosslinks (Table S2) were used to test these structures, with no predicted structure satisfying all the observed crosslinks (Figure 1b–d, Table S3). In all three models, the K144–K342 distance is too long, with the remaining modeling violations involving PBD. The K6–K144 crosslink is not satisfied for the AlphaFold2 and RoseTTAFold PBD, which are both by the catalytic residues. Additionally, the RoseTTAFold structure cannot satisfy the K6–K62 crosslink. In contrast, the I-TASSER PBD satisfies both sets of crosslinks, but not the K6–K80. These observations suggest that either PBD binds to a site other than the predicted ones or that the XL-MS data are sampling multiple PBD conformational states.

2.3 | Multiple PBD binding orientations observed during HADDOCK docking

Multiple PBD conformational states were predicted by the HADDOCK docking program depending on initial PBD positions, distance restraints, flexibility of residues, and ambiguous restraints (Table S4 and Table S9). HADDOCK allows ambiguous distance restraints, meaning that during model minimization, HADDOCK may eliminate restraints, which can be useful when sampling multiple conformations.^{37,38} Altering the initial PBD position (Figure S4a and Table S4 *test 1*) between the AlphaFold2, I-TASSER, or a remote site changes the distribution of PBD conformations between the AlphaFold2 and I-TASSER sites, as well as a site in between (mid site) (Figure S4b). Based on observed PBD crosslinks, flexible residues and 11 ambiguous distance restraints were used to explore the possibility of multiple PBD conformations. HADDOCK treats PBD as separate from the rest of PTEN, so an unambiguous distance restraint was added between the “cut” ends. When it is modeled as an α -helix with a flexible linker (residues 11–22), the AlphaFold2 and mid sites are favored (Figure S4f and Table S4 *test 5*). PBD at the mid site satisfies more of the crosslinks than when it was at the AlphaFold2 site (Table S5), which suggests the mid site as a possible PBD binding orientation. If residues 1–24 are flexible (Table S4 *test 6*), PBD favors both the I-TASSER and AlphaFold2 positions, which supports the PBD binding multistate model. PBD at the AlphaFold2 orientation favors an α -helical conformation and the I-TASSER orientation is more disordered (Figure 2a, S6 and S7).

2.4 | Rosetta modeling supports the multistate PBD binding orientation hypothesis

Rosetta modeling can incorporate experimental restraints^{39–41} and model interdomain interactions. As with HADDOCK, the choice of initial structure and how the restraints are applied can affect the final model (Figure S2 for Rosetta convergence and Table S9 for model quality assessment). When the initial I-TASSER structure and the full 31 restraint set were used, the three lowest energy structures have extended α -helices near the initial I-TASSER PBD binding site, but oriented at a different angle (Figure 2b). When the AlphaFold2 model and full restraint set were used, the final models were similar to the initial PBD binding (Figure 2c). The AlphaFold2 model did not satisfy the K6–K144 and K144–K342 crosslinks, while the I-TASSER model did not satisfy the K6–K80, K6–K327, and K144–K342 crosslinks (Figure 1b, Table S3). We used limited restraint sets to explore the possibility of multiple PBD binding states. One set used the I-TASSER model as an initial structure, but excluded the K6–K80, K6–K327, K6–K330, and K6–K330 restraints (Table S8c). The I-TASSER-based simulation with this set still produced an extended helix, but two of the lowest energy structures have a kink that align them with the initial I-TASSER PBD orientation (Figure 2d). The final set used the AlphaFold2 model as an initial structure but excluded the K6–K144 and K144–K342 restraints (Table S8d). This simulation resulted in more variability in the final orientation than the other simulations (Figure 2e), which is interesting given the variation in binding near the catalytic residues by the AlphaFold2 and RoseTTAFold models and the 7JUL structure.

2.5 | Inter-residue cross-correlation of PBD K13–D24 salt-bridge reveals cooperative and competitive interaction sites

The PBD activates PTEN phosphatase function,^{5,7,8} suggesting coupling between it and the catalytic/active site. We used the CONTACT ANALYSIS (CONAN) tool⁴² to analyze the time course of molecular dynamics simulations and explore PTEN inter-residue contacts and dynamics. In the I-TASSER model, PBD is distal from the active site, whereas it is packed against the active site in both the AlphaFold2 and RoseTTAFold models (Figures 1a and 3), demonstrating that it explores multiple states. The AlphaFold2 site is the most variable within its biggest structural cluster and between MD

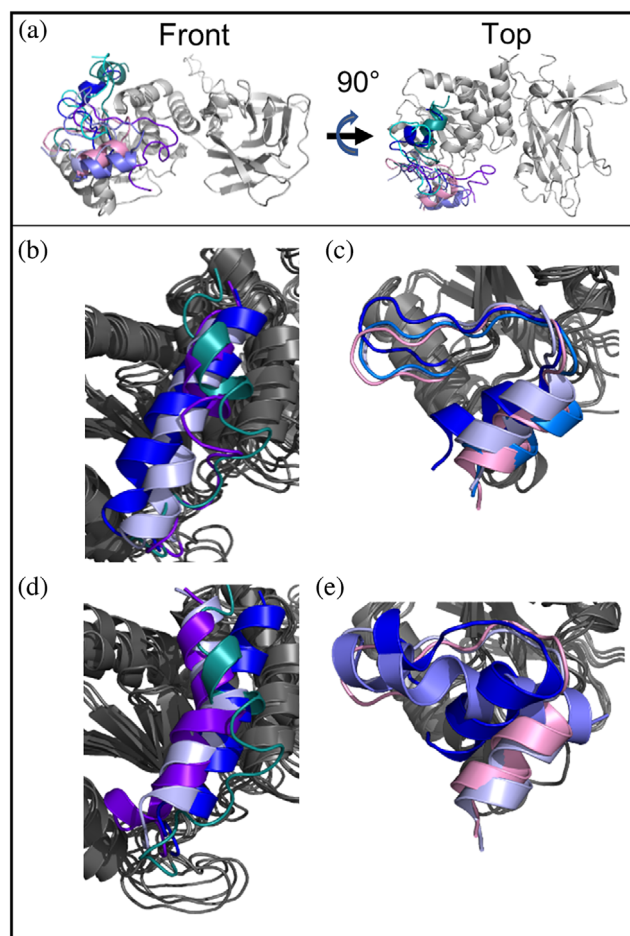


FIGURE 2 Integrative modeling of PTEN PBD and PD-C2 using crosslinking, HADDOCK and Rosetta. (a) Docking of PTEN PBD and PD-C2 with HADDOCK and experimental crosslinks. The docked PBD are shown in various shades of blue overlaid onto the PD-C2 superdomain (in gray). Each PBD represents one of five of the lowest energy clusters from HADDOCK docking (Table S4 *test 6*). The AlphaFold2 and I-TASSER PBD are shown as reference in pink and teal, respectively. The docked PBD sample both the AlphaFold2 and I-TASSER predicted binding sites with the PBD at the AlphaFold2 site displaying more α -helical propensity. (b,c) Intermolecular binding between PBD and PD-C2 using Rosetta Comparative Modeling. (b) Modeling PBD interactions with all 31 observed crosslinks (Table S2) using I-TASSER PTEN structure as the initial structure (PBD shown in teal). The PBD from the three lowest energy structures from Rosetta were overlaid in blue. (c) Modeling PBD interactions with all 31 observed crosslinks using AlphaFold2 PTEN structure with the initial PBD orientation in pink and the lowest energy structures in blue. (d,e) Modeling a two-state PBD model. Neither the AlphaFold2 nor the ITASSER PTEN structures satisfy all of the observed crosslinks (Figure 1b–d, Table S3). Here, we test if crosslinking observes exchange between two sites using Rosetta modeling with a limited set of crosslinks to constrain binding to one or another site. (d) Starting from the I-TASSER structure (teal). (e) Starting from the AlphaFold2 structure (pink). The modeled PBD in shades of blue

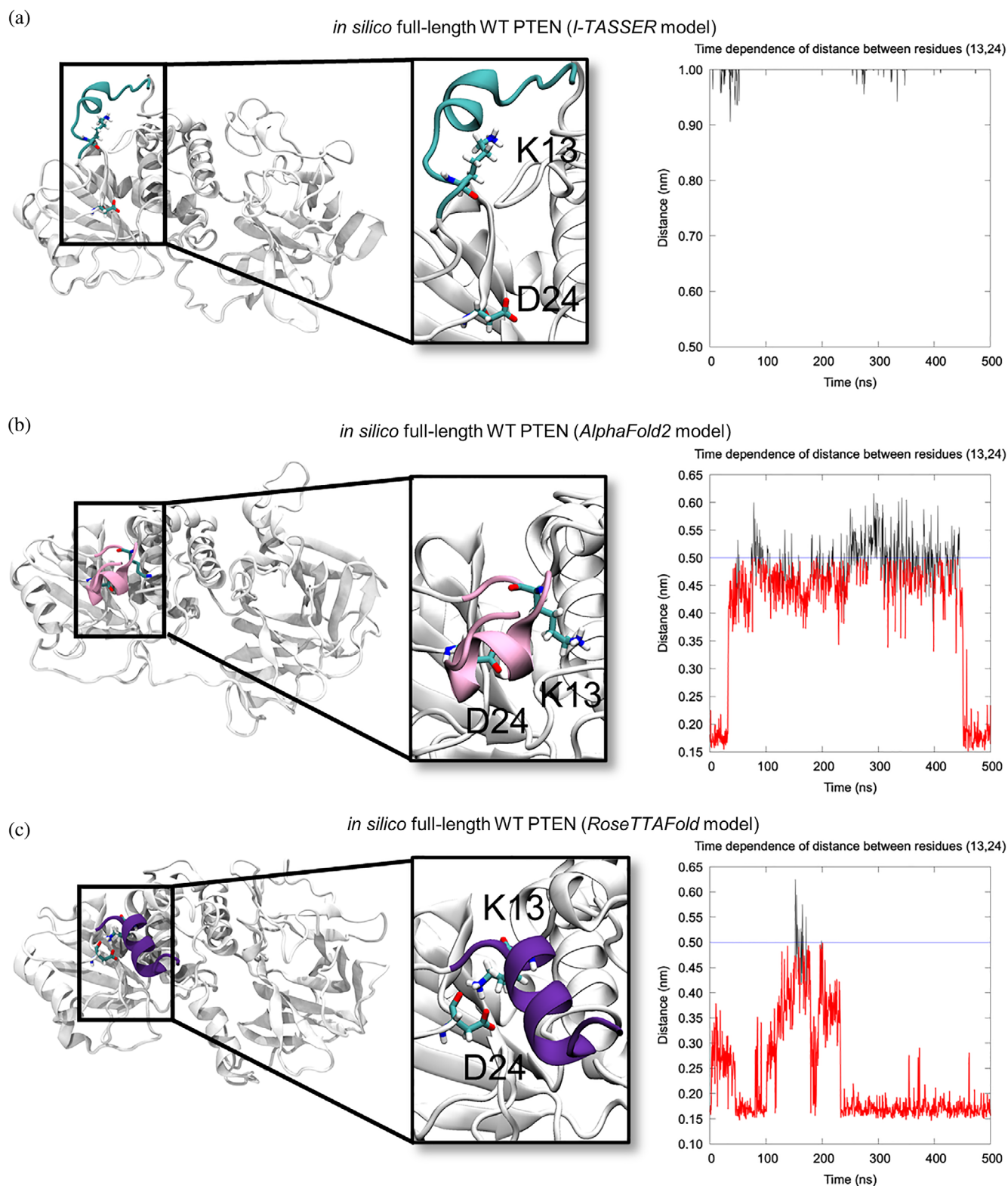


FIGURE 3 PBD intra-molecular interaction analysis for full-length WT PTEN structure. Interaction between amino acid residues K13–D24 for the (a) *I-TASSER* (top inset), (b) *AlphaFold2* (middle inset), and (c) *RoseTTAFold* (bottom inset) models. PBD conformations (left panel) are colored in cyan, pink, and purple for the *I-TASSER*, *AlphaFold2*, and *RoseTTAFold* models, respectively. The K13 and D24 amino acid residues involved in salt-bridge interaction are depicted in licorice representation. The time evolution and forming of a salt-bridge between K13 and D24 is shown in the right panel

replicates (Figures S5 and S6). Residue K13 is important for PIP₂ binding and PTEN activation.^{9,13} The distance between residues K13 and D24 was used to distinguish between PBD conformational states and probe inter-residue contacts (Figure S7, *left* panels). These residues are close in the AlphaFold2 model, likely forming a salt-bridge. In the I-TASSER model, the distance between K13 and D24 is considerably larger, with brief periods close to each other, making interaction unlikely (Figure 3 and Figure S7a *left* panel). The PTEN active site is formed by the TI, WPD, and P loops. In the AlphaFold2 model, the intrinsically disordered region and active site TI loop positively correlate with PBD residues K13–D24 and behave in a cooperative manner (Figure S7b, *right* panel). In contrast, in the RoseTTAFold model, active site residues (in P and WPD loops) behave in a competitive manner (Figure S7c, *right* panel). These interaction patterns suggest that different PBD orientations have distinct consequences to the PTEN active site. A “control” MD simulation of truncated PTEN missing the PBD (delPBD) reveals how its absence greatly diminishes correlative active site inter-residue contacts (Figure S7d).

2.6 | PBD conformational changes correlates with dynamic regions and influence communication in the active site

To identify critical residues that communicate PBD conformational changes within PTEN, we examined the residue interaction network (RIN) connectivity in PBD and catalytic residues. RINs have been utilized to identify critical nodes (residues), which have a high degree of connectivity (>4 edges, interactions)⁴³ and are crucial for structural stability, signal propagation, and protein function.⁴⁴ The RIN distributions reveal distinct connectivity differences between the PBD and active site in each of the predicted models. This might be, in part, due to cooperative conformational dynamics formed between PBD residues K13 and D24 and highly conserved residues within the active site (C124 and R130), suggesting rapid signal propagation through a small network of core residues. For the active site residues, R130 is a hub residue in all models with a high degree of network connectivity (Figure S7, *middle* panels), but decreased connectivity is seen for R130 in the AlphaFold2 model (Figure S7b, *middle* panel). A decrease in connectivity is seen in residues R130 and C124 in the delPBD PTEN “control” model, suggesting that deletion of the PBD diminishes signal propagation and possible catalytic function. M134 is a critical active site hub residue in AlphaFold2 and RoseTTAFold models, but not the I-TASSER model, suggesting that, while M134 plays a role in functional

signal transmission, a shift in PBD conformation changes its importance in PTEN communication networks (Figure S7b and 7c, *middle* and *right* panels). Changes in connectivity that disrupt these interactions would also disrupt overall PTEN function. Our results suggest that PBD residues have cooperative conformational dynamics and strong connectivity for active site residues, identifying them as critical hubs for signal propagation.

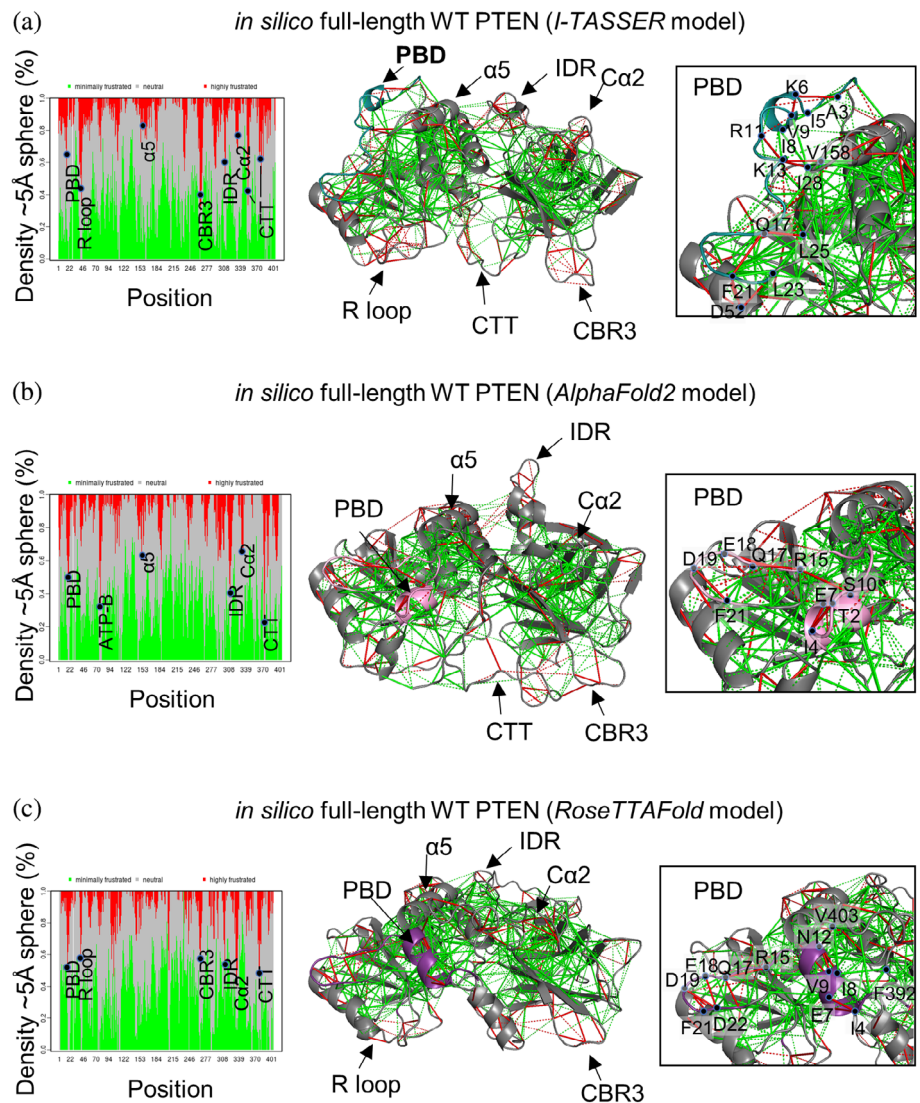
Disordered proteins often display many conformational substates explained by a rugged energy landscape, allowing multiple binding modes.⁴⁵ Protein “energetic frustration” is a useful concept for predicting locally dynamic regions^{46–49} in the predicted structures. To sample the PTEN free energy landscape,⁴⁹ we applied a frustratometer algorithm^{46–48} to quantify the residual local frustration in the predicted structures. Each predicted PTEN structure displays different PBD frustration patterns, stabilized by conformation-specific frustration interactions, but PBD regions are highly frustrated regions within each of the models (Figure 4 *right* panels), which suggests it is a critical functional region. Regions where large-scale conformational changes occur are often enriched in patches of highly frustrated interactions, thereby identifying regions that influence protein function.⁴⁶

3 | DISCUSSION

The recent success of integrative structural biology approaches, including AlphaFold2 structure prediction,²⁴ has led to considerable discussion and excitement for the future of structure prediction and determination.⁵⁰ Our integrative structural approach, incorporating experimental crosslinks with *in silico* methods, identified multiple PBD states for the full-length WT PTEN. A recent X-ray structure¹⁸ [PBDID 7JUL] was consistent with the RoseTTAFold prediction. None of the predicted models satisfy all crosslinks, suggesting either incorrect predictions by the algorithms or the presence of multiple orientations of this domain. HADDOCK models suggest that PBD is α -helical near the active site of PTEN and more disordered at other sites. The MD simulations and frustration metrics⁴⁸ reveal that it exists in a disordered state with exchange between multiple conformations.

PBD conformational position affects the catalytic residues, suggesting a mechanism explaining the low- and high-activity catalytic states.¹³ In the AlphaFold2 and RoseTTAFold models, it is proximal to the active site and their residues are communication hubs connecting them to other residues. It is distal to the active site in the I-TASSER model, located in a patch of hydrophobic and aromatic residues, and its interaction network is a larger

FIGURE 4 Local frustration in full-length WT PTEN structure. Projection plot of local frustration distributions along the sequence (left panel), local frustration patterns across structure (middle panel), and PBD local frustration patterns depicting residue interactions (right inset panel) for (a) I-TASSER, (b) AlphaFold2, and (c) RoseTTAFold models. The local frustration patterns of the full-length WT PTEN protein, with the minimally frustrated interactions shown in green, neutral contacts shown in gray, and highly frustrated interactions are shown in red. The backbones of the proteins are shown as gray cartoons, minimally frustrated contacts are depicted with green lines, highly frustrated interactions are depicted with red lines. Neutral interactions were omitted for clarity. Highly frustrated areas in projection plot are indicated in black spheres



cluster of residues more suggestive of a binding site. Residue M134 is a critical active site hub residue in the AlphaFold2 and RoseTTAFold model, but not in the I-TASSER model. M134 mutations result in compromised lipid phosphatase activity^{51–53} and are associated with breast cancer⁵² and Bannayan–Riley–Ruvalcaba syndrome,^{52,54} supporting the functional importance of this residue. Moreover, PBD conformations affect the electrostatic distribution at the active site, potentially changing the binding of the negatively charged PIP₃ (Figure S8). PBD mutations can have complex consequences to phosphatase function. For example, K13A PTEN has decreased phosphatase function *in vitro*,^{5,13,55} but binds PIP₂ and functions *in vivo*.^{7,55,56} Taken together, our results represent an important step in integrative structural modeling, especially the use of next generation structure prediction methods, which provide a potential structural explanation for PTEN activation by PIP₂.

4 | MATERIALS AND METHODS

The Materials and Methods are presented in full detail in the Supplementary Materials. In brief, full-length wild-type (WT) human PTEN (residues 1–403) was expressed with a C-terminal 6-His tag (a gift from Alonzo Ross [addgene plasmid #20741])⁵⁷ and purified using a modified protocol (Redfern et al.,⁵⁷ Johnston and Raines⁵⁸). The full-length PTEN models were predicted using AlphaFold2,^{24,26} RoseTTAFold,²⁷ and I-TASSER (as previously described²¹). PBD orientation reproducibility and model quality assessment (pLDDT^{59,60}) are shown in Figure S1 and Table S1. WT PTEN crosslinking was done with DSSO (Lys–Lys) and BMSO (Cys–Cys) crosslinkers using previously described protocols (Khan et al.,^{61,62} Klykov et al.,⁶³ Gutierrez et al.⁶⁴). Crosslinking-based restraints were incorporated into PTEN models using the HADDOCK 2.4 webserver^{64,65} and the Rosetta Comparative Modeling protocol.⁶⁶ Model quality

assessments are listed in Table S9. Binding interface and sequence conservation predictions were aided by the CPORT³² and ConSurf²⁸ programs, respectively. All-atom molecular dynamics (MD) simulations were conducted using GROMACS 2018.2 software⁶⁷ with CHARMM36m forcefield.⁶⁸ The MD simulations were analyzed utilizing the GROMOS clustering algorithm,⁶⁹ inter-residue CONTACT ANALYSIS (CONAN),⁴² Residue Interaction Network (RIN) analysis,⁷⁰ and residual local frustration analysis.⁴⁶

ACKNOWLEDGMENTS

We thank Ann Tushar for her assistance in protein sample preparation, as well as Hyunbum Jang and Ruth Nussinov for their critical review of the manuscript. This work was funded, in part, by the Ambrose Monell Foundation PTEN-Switch Grant, a grant allocation of computing time from the Ohio Supercomputing Center (PCCF0020) [both to C.E.], and the National Institute of Aging (NIA) under Award Number U01AG073323 and R01AG066707 (both to F.C.). I.N.S. is funded, in part, by the Ambrose Monell Cancer Genomic Medicine Fellowship and National Institutes of Health (NIH)/National Institute of General Medical Sciences (NIGMS) Maximizing Opportunities for Scientific and Academic Independent Careers (MOSAIC) K99/R00 Grant—1K99GM143552-01. C.E. is an American Cancer Society Clinical Research Professor and the Sondra J. and Stephen R. Hardis Endowed Chair of Cancer Genomic Medicine at the Cleveland Clinic. The ThermoFisher Scientific Fusion Lumos Tribrid mass spectrometer was purchased via an NIH shared instrument grant (1S10OD023436-01). The HADDOCK docking program requested that the following acknowledgment be made: The FP7 WeNMR (project# 261572), H2020 West-Life (project# 675858), the EOSC-hub (project# 777536), and the EGI-ACE (project# 101017567) European e-Infrastructure projects are acknowledged for the use of their web portals, which make use of the EGI infrastructure with the dedicated support of CESNET-MCC, INFN-PADOVA-STACK, INFN-LNL-2, NCG-INGRID-PT, TW-NCHC, CESGA, IFCA-LCG2, UA-BITP, SURFsara, and NIKHEF, and the additional support of the National GRID Initiatives of Belgium, France, Italy, Germany, the Netherlands, Poland, Portugal, Spain, UK, Taiwan, and the US Open Science Grid.

AUTHOR CONTRIBUTIONS

Jennifer E. Dawson: Conceptualization (equal); data curation (equal); formal analysis (equal); investigation (equal); methodology (equal); validation (equal); visualization (lead); writing – original draft (lead); writing – review and editing (supporting). **Iris Nira Smith:** Conceptualization (equal); data curation (equal); formal analysis (equal);

funding acquisition (supporting); investigation (equal); methodology (equal); validation (equal); visualization (supporting); writing – original draft (supporting); writing – review and editing (supporting). **William Martin:** Data curation (supporting); investigation (supporting); software (supporting); validation (supporting); writing – review and editing (supporting). **Krishnendu Khan:** Methodology (supporting); resources (supporting); validation (supporting); writing – review and editing (supporting). **Feixiong Cheng:** Funding acquisition (supporting); validation (supporting); writing – review and editing (supporting). **Charis Eng:** Conceptualization (equal); funding acquisition (lead); project administration (lead); supervision (lead); validation (supporting); writing – review and editing (supporting).

ORCID

Jennifer E. Dawson  <https://orcid.org/0000-0002-8387-6109>

Iris Nira Smith  <https://orcid.org/0000-0001-5560-8871>

Krishnendu Khan  <https://orcid.org/0000-0001-7666-1030>

Feixiong Cheng  <https://orcid.org/0000-0002-1736-2847>

Charis Eng  <https://orcid.org/0000-0002-3693-5145>

REFERENCES

- Liu T, Wang Y, Wang Y, Chan AM. Multifaceted regulation of PTEN subcellular distributions and biological functions. *Cancers (Basel)*. 2019;11(9):1247.
- Yehia L, Ngeow J, Eng C. PTEN-opathies: From biological insights to evidence-based precision medicine. *J Clin Invest*. 2019;129(2):452–464.
- Carnero A, Paramio JM. The pten/pi3k/akt pathway in vivo, cancer mouse models. *Front Oncol*. 2014;4:252.
- Yin Y, Shen WH. Pten: A new guardian of the genome. *Oncogene*. 2008;27(41):5443–5453.
- Campbell RB, Liu F, Ross AH. Allosteric activation of pten phosphatase by phosphatidylinositol 4,5-bisphosphate. *J Biol Chem*. 2003;278(36):33617–33620.
- Martin TF. Phosphoinositide lipids as signaling molecules: Common themes for signal transduction, cytoskeletal regulation, and membrane trafficking. *Annu Rev Cell Dev Biol*. 1998;14:231–264.
- Gil A, Rodriguez-Escudero I, Stumpf M, Molina M, Cid VJ, Pulido R. A functional dissection of pten n-terminus: Implications in pten subcellular targeting and tumor suppressor activity. *PLoS One*. 2015;10(4):e0119287.
- Duerr EM, Rollbrocker B, Hayashi Y, et al. Pten mutations in gliomas and glioneuronal tumors. *Oncogene*. 1998;16(17):2259–2264.
- Das S, Dixon JE, Cho W. Membrane-binding and activation mechanism of pten. *Proc Natl Acad Sci USA*. 2003;100(13):7491–7496.
- Yeung T, Terebiznik M, Yu L, et al. Receptor activation alters inner surface potential during phagocytosis. *Science*. 2006;313(5785):347–351.

11. McConnachie G, Pass I, Walker SM, Downes CP. Interfacial kinetic analysis of the tumour suppressor phosphatase, pten: Evidence for activation by anionic phospholipids. *Biochem J*. 2003;371(Pt 3):947–955.
12. Leslie NR, Batty IH, Maccario H, Davidson L, Downes CP. Understanding pten regulation: Pip2, polarity and protein stability. *Oncogene*. 2008;27(41):5464–5476.
13. Johnston SB, Raines RT. Catalysis by the tumor-suppressor enzymes pten and pten-l. *PLoS One*. 2015;10(1):e0116898.
14. Malaney P, Pathak RR, Xue B, Uversky VN, Dave V. Intrinsic disorder in pten and its interactome confers structural plasticity and functional versatility. *Sci Rep*. 2013;3:2035.
15. Malaney P, Uversky VN, Dave V. Identification of intrinsically disordered regions in pten and delineation of its function via a network approach. *Methods*. 2015;77-78:69–74.
16. Lee CU, Hahne G, Hanske J, et al. Redox modulation of pten phosphatase activity by hydrogen peroxide and bisperoxidovanadium complexes. *Angew Chem Int Ed Engl*. 2015;54(46):13796–13800.
17. Lee JO, Yang H, Georgescu MM, et al. Crystal structure of the pten tumor suppressor: Implications for its phosphoinositide phosphatase activity and membrane association. *Cell*. 1999;99(3):323–334.
18. Dempsey DR, Viennet T, Iwase R, et al. The structural basis of pten regulation by multi-site phosphorylation. *Nat Struct Mol Biol*. 2021;28(10):858–868.
19. Bullock JMA, Sen N, Thalassinos K, Topf M. Modeling protein complexes using restraints from crosslinking mass spectrometry. *Structure*. 2018;26(7):1015–1024.e1012.
20. Braitbard M, Schneidman-Duhovny D, Kalisman N. Integrative structure modeling: Overview and assessment. *Annu Rev Biochem*. 2019;88:113–135.
21. Jang H, Smith IN, Eng C, Nussinov R. The mechanism of full activation of tumor suppressor pten at the phosphoinositide-enriched membrane. *iScience*. 2021;24(5):102438.
22. Yang J, Zhang Y. I-tasser server: New development for protein structure and function predictions. *Nucleic Acids Res*. 2015;43(W1):W174–W181.
23. Zhang C, Freddolino PL, Zhang Y. Cofactor: Improved protein function prediction by combining structure, sequence and protein-protein interaction information. *Nucleic Acids Res*. 2017;45(W1):W291–W299.
24. Jumper J, Evans R, Pritzel A, et al. Highly accurate protein structure prediction with alphafold. *Nature*. 2021;596(7873):583–589.
25. Varadi M, Anyango S, Deshpande M, et al. Alphafold protein structure database: Massively expanding the structural coverage of protein-sequence space with high-accuracy models. *Nucleic Acids Res*. 2021;50(D1):D439–D444.
26. Mirdita MSK, Moriwaki Y, Heo L, Ovchinnikov S, Steinegger M. Colabfold—making protein folding accessible to all. *bioRxiv*. 2021. <https://doi.org/10.1101/2021.08.15.456425>
27. Baek M, DiMaio F, Anishchenko I, et al. Accurate prediction of protein structures and interactions using a three-track neural network. *Science*. 2021;373(6557):871–876.
28. Ashkenazy H, Abadi S, Martz E, et al. Consurf 2016: An improved methodology to estimate and visualize evolutionary conservation in macromolecules. *Nucleic Acids Res*. 2016;44(W1):W344–W350.
29. Ashkenazy H, Erez E, Martz E, Pupko T, Ben-Tal N. Consurf 2010: Calculating evolutionary conservation in sequence and structure of proteins and nucleic acids. *Nucleic Acids Res*. 2010;38:W529–W533.
30. Glaser F, Pupko T, Paz I, et al. Consurf: Identification of functional regions in proteins by surface-mapping of phylogenetic information. *Bioinformatics*. 2003;19(1):163–164.
31. Landau M, Mayrose I, Rosenberg Y, et al. Consurf 2005: The projection of evolutionary conservation scores of residues on protein structures. *Nucleic Acids Res*. 2005;33:W299–W302.
32. de Vries SJ, Bonvin AM. Cport: A consensus interface predictor and its performance in prediction-driven docking with haddock. *PLoS One*. 2011;6(3):e17695.
33. Kao A, Chiu CL, Vellucci D, et al. Development of a novel cross-linking strategy for fast and accurate identification of cross-linked peptides of protein complexes. *Mol Cell Proteomics*. 2011;10(1):M110, 002212.
34. Gutierrez CB, Block SA, Yu C, et al. Development of a novel sulfoxide-containing ms-cleavable homobifunctional cysteine-reactive cross-linker for studying protein-protein interactions. *Anal Chem*. 2018;90(12):7600–7607.
35. Gutierrez CB, Yu C, Novitsky EJ, Huszagh AS, Rychnovsky SD, Huang L. Developing an acidic residue reactive and sulfoxide-containing ms-cleavable homobifunctional cross-linker for probing protein-protein interactions. *Anal Chem*. 2016;88(16):8315–8322.
36. Gutierrez C, Chemmama IE, Mao H, et al. Structural dynamics of the human cop9 signalosome revealed by cross-linking mass spectrometry and integrative modeling. *Proc Natl Acad Sci U S A*. 2020;117(8):4088–4098.
37. Orban-Nemeth Z, Beveridge R, Hollenstein DM, et al. Structural prediction of protein models using distance restraints derived from cross-linking mass spectrometry data. *Nat Protoc*. 2018;13(3):478–494.
38. Bonvin A, Karaca E, Kastiris PL, Rodrigues J. Defining distance restraints in haddock. *Nat Protoc*. 2018;13(7):1503.
39. Kahraman A, Herzog F, Leitner A, Rosenberger G, Aebersold R, Malmstrom L. Cross-link guided molecular modeling with rosetta. *PLoS One*. 2013;8(9):e73411.
40. Lossl P, Kolbel K, Tanzler D, et al. Analysis of nidogen-1/laminin gamma1 interaction by cross-linking, mass spectrometry, and computational modeling reveals multiple binding modes. *PLoS One*. 2014;9(11):e112886.
41. Mintseris J, Gygi SP. High-density chemical cross-linking for modeling protein interactions. *Proc Natl Acad Sci USA*. 2020;117(1):93–102.
42. Mercadante D, Grater F, Daday C. Conan: A tool to decode dynamical information from molecular interaction maps. *Biophys J*. 2018;114(6):1267–1273.
43. Vishveshwara S, Ghosh A, Hansia P. Intra and inter-molecular communications through protein structure network. *Curr Protein Pept Sci*. 2009;10(2):146–160.
44. Bode C, Kovacs IA, Szalay MS, Palotai R, Korcsmaros T, Csermely P. Network analysis of protein dynamics. *FEBS Lett*. 2007;581(15):2776–2782.
45. Tompa P, Fuxreiter M. Fuzzy complexes: Polymorphism and structural disorder in protein-protein interactions. *Trends Biochem Sci*. 2008;33(1):2–8.

46. Ferreiro DU, Hegler JA, Komives EA, Wolynes PG. Localizing frustration in native proteins and protein assemblies. *Proc Natl Acad Sci U S A*. 2007;104(50):19819–19824.
47. Rausch AO, Freiburger MI, Leonetti CO, et al. Frustratometer: An r-package to compute local frustration in protein structures, point mutants and md simulations. *Bioinformatics*. 2021;37(18):3038–3040.
48. Gianni S, Freiburger MI, Jemth P, Ferreiro DU, Wolynes PG, Fuxreiter M. Fuzziness and frustration in the energy landscape of protein folding, function, and assembly. *Acc Chem Res*. 2021;54(5):1251–1259.
49. Freiburger MI, Wolynes PG, Ferreiro DU, Fuxreiter M. Frustration in fuzzy protein complexes leads to interaction versatility. *J Phys Chem B*. 2021;125(10):2513–2520.
50. Masrati G, Landau M, Ben-Tal N, Lupas A, Kosloff M, Kosinski J. Integrative structural biology in the era of accurate structure prediction. *J Mol Biol*. 2021;433(20):167127.
51. Mighell TL, Evans-Dutson S, O’Roak BJ. A saturation mutagenesis approach to understanding pten lipid phosphatase activity and genotype-phenotype relationships. *Am J Hum Genet*. 2018;102(5):943–955.
52. Figer A, Kaplan A, Frydman M, et al. Germline mutations in the pten gene in israeli patients with bannayan-riley-ruvalcaba syndrome and women with familial breast cancer. *Clin Genet*. 2002;62(4):298–302.
53. Post KL, Belmadani M, Ganguly P, et al. Multi-model functionalization of disease-associated pten missense mutations identifies multiple molecular mechanisms underlying protein dysfunction. *Nat Commun*. 2020;11(1):2073.
54. Garcia-Garcia MJ, Eggenschwiler JT, Caspary T, et al. Analysis of mouse embryonic patterning and morphogenesis by forward genetics. *Proc Natl Acad Sci U S A*. 2005;102(17):5913–5919.
55. Nguyen HN, Yang JM, Miyamoto T, et al. Opening the conformation is a master switch for the dual localization and phosphatase activity of pten. *Sci Rep*. 2015;5:12600.
56. Mighell TL, Thacker S, Fombonne E, Eng C, O’Roak BJ. An integrated deep-mutational-scanning approach provides clinical insights on pten genotype-phenotype relationships. *Am J Hum Genet*. 2020;106(6):818–829.
57. Redfern RE, Redfern D, Furgason ML, Munson M, Ross AH, Gericke A. Pten phosphatase selectively binds phosphoinositides and undergoes structural changes. *Biochemistry*. 2008;47(7):2162–2171.
58. Johnston SB, Raines RT. Conformational stability and catalytic activity of pten variants linked to cancers and autism spectrum disorders. *Biochemistry*. 2015;54(7):1576–1582.
59. Tunyasuvunakool K, Adler J, Wu Z, et al. Highly accurate protein structure prediction for the human proteome. *Nature*. 2021;596(7873):590–596.
60. Mariani V, Biasini M, Barbato A, Schwede T. Lddt: A local superposition-free score for comparing protein structures and models using distance difference tests. *Bioinformatics*. 2013;29(21):2722–2728.
61. Khan K, Baleanu-Gogonea C, Willard B, Gogonea V, Fox PL. 3-Dimensional architecture of the human multi-trna synthetase complex. *Nucleic Acids Res*. 2020;48(15):8740–8754.
62. Khan K, Baleanu-Gogonea C, Willard B, Gogonea V, Fox P. An optimized protocol for in vitro and in cellulo structural determination of the multi-trna synthetase complex by cross-linking mass spectrometry. *Star Protoc*. 2022;3:101201.
63. Klykov O, Steigenberger B, Pektas S, Fasci D, Heck AJR, Scheltema RA. Efficient and robust proteome-wide approaches for cross-linking mass spectrometry. *Nat Protoc*. 2018;13(12):2964–2990.
64. Honorato RV, Koukos PI, Jimenez-Garcia B, et al. Structural biology in the clouds: The wenmr-eosc ecosystem. *Front Mol Biosci*. 2021;8:729513.
65. van Zundert GCP, Rodrigues J, Trellet M, et al. The haddock2.2 web server: User-friendly integrative modeling of biomolecular complexes. *J Mol Biol*. 2016;428(4):720–725.
66. Song Y, DiMaio F, Wang RY, et al. High-resolution comparative modeling with rosetta-cm. *Structure*. 2013;21(10):1735–1742.
67. Abraham MJ, Murtola T, Schulz R, et al. Gromacs: High performance molecular simulations through multi-level parallelism from laptops to supercomputers. *SoftwareX*. 2015;1–2:19–25.
68. Huang J, Rauscher S, Nawrocki G, et al. Charmm36m: An improved force field for folded and intrinsically disordered proteins. *Nat Methods*. 2017;14(1):71–73.
69. Daura X, Gademann K, Juan B, Seebach D, van Gunsteren WF, Mark AE. Peptide folding: When simulation meets experiment. *Angew Chem Int Ed*. 1999;38:236–240.
70. Piovesan D, Minervini G, Tosatto SC. The ring 2.0 web server for high quality residue interaction networks. *Nucleic Acids Res*. 2016;44(W1):W367–W374.

SUPPORTING INFORMATION

Additional supporting information may be found in the online version of the article at the publisher’s website.

How to cite this article: Dawson JE, Smith IN, Martin W, Khan K, Cheng F, Eng C. Shape shifting: The multiple conformational substates of the PTEN N-terminal PIP₂-binding domain. *Protein Science*. 2022;31(5):e4308. <https://doi.org/10.1002/pro.4308>